# Quantitative depth-profile analysis of transition metal nitride materials with combined grazing-incidence X-ray fluorescence and X-ray reflectometry analysis

S. Torrengo, D. Eichert, Y. Mazel, M. Bernard, Yves Ménesguen, Marie-Christine Lépy, E. Nolot

# Quantitative depth-profile analysis of transition metal nitride materials with combined grazing-incidence X-ray fluorescence and X-ray reflectometry analysis

S. Torrengo[1*], D. Eichert[2], Y. Mazel[1], M. Bernard[1], Y. Ménesguen[3], M.C. Lépy[3], E. Nolot[1]

*(1) Univ. Grenoble Alpes, CEA, LETI, F-38000, Grenoble, France*
*(2) ELETTRA Sincrotrone Trieste, Area Science Park, S.S. 14 – Km 163, 5, 34149 Basovizza Trieste, Italy*
*(3) CEA, LIST, Laboratoire National Henri Becquerel, 91191 Gif-sur-Yvette, France*

**simona.torrengo@cea.fr*

## Abstract

Refractory transition metal nitrides are attracting attention in many microelectronics research and development fields. Their different applications and desired performances require a precise control of the film thickness and elemental depth profile. This information can be non-destructively obtained combining Grazing-Incidence X-ray Fluorescence (GIXRF) and X-ray Reflectometry (XRR) analysis. GIXRF-XRR joint analysis can be performed following a reference-free approach, which requires the knowledge of the whole experimental system. However, such a rigorous metrological approach cannot be easily applied to in-lab or in-fab tools due to the difficulty to access the various experimental set-up parameters, therefore another approach is needed.

In this paper, we used a reference-based method consisting in the use of known standard samples, close in composition and structure from the samples to analyze, to deduce the key parameters of the instrumental setup, which are then used to perform quantitative GIXRF-XRR combined analysis of the samples of interest. We applied this method to titanium tungsten nitride thin films elaborated by Physical Vapor Deposition (PVD). Our results show that the reference-based method, using carefully determined instrumental functions, can meet the requirement for both qualitative and quantitative depth-profiling analysis, being in addition more easily to implement into labs and fabs than the reference-free method.

**Author Keywords:** Grazing-incidence X-ray fluorescence; X-ray Reflectometry; Plasma profiling Time-of-flight mass spectrometry; elemental depth profiling; quantitative analysis.

## 1. Introduction

TiN materials have been applied in microelectronics since some time due to their low resistance, but it is only in recent years that refractory transition metal nitrides such as titanium tungsten nitride (TiWN) and tungsten nitride (WN) have attracted attention. These nitrides could find applications in microelectronics as contacts on n-doped semiconductor materials for the implementation of Schottky contacts [1-5], as tunable heater inside Phase Change Random Access Memory [6], as resistors in IR projectors [7] or as diffusion barrier [8-11]. The desired functionality of these materials, similarly to number of other nanoscaled materials, can be obtained by a variation of their spatial or elemental composition [7-9], often involving multi-layered structures [2] or elemental depth profiles [10]. However, the practical implementation of multi-layered structures requires a precise control of their film thickness and composition, thus pushing the research towards the development of new non-destructive characterization techniques compatible with fabrication facilities.

Recently the combination of two techniques, X-ray Reflectometry (XRR) and Grazing-Incidence X-ray Fluorescence (GIXRF) has become a strong candidate to answer this need [12-22].

XRR is a non-destructive characterization technique widely used in in-fab laboratory to determine thickness, roughness and mass density of thin films for thicknesses ranging from a few nanometers to some hundreds of nanometers, as well as the optical properties of the reflecting surface and interfaces [23]. The technique consists in the measure of the intensity of a reflected monochromatic X-ray beam in the specular direction while varying its incidence angle near the critical angle of total external reflection. When the interface between the film and the substrate is not perfectly sharp, *i.e.* presents an average mass density profile, the specular reflected intensity deviates from the Fresnel's law reflectivity prediction. The reflectivity curve shape can be brought back to the mass density profile normal to the surface, to the layers thickness and to the interfaces roughness [24]. The technique uses the average mass density of a layer as a variable and thus cannot provide information on its elemental composition. Therefore, prior knowledge of the elemental composition of each layer is necessary to obtain their related elemental mass compositionfrom XRR data.

Instead, GIXRF is a powerful non-destructive characterization technique for elemental depth profiling of thin layers up to a few hundred nanometers, giving access the elemental distribution and related doses [25-29]. The GIXRF technique is based on the measurement of the fluorescence signal emitted by the elements present in the sample as a function of the X-ray grazing incidence angle. In this range, the incident and the reflected beams interfere to create an X-ray Standing Wave (XSW) field with locally dependent electric field modulations [30,31]. The emitted fluorescence signal is dependent on the intensity of the XSW field at a given depth and therefore on the atomic distribution over the overall thickness. However, this technique does not provide an unambiguous depth profile reconstruction in terms of mass density and thickness.

A combined GIXRF and XRR analysis is possible and has already been identified to be a promising methodological approach to reliably characterize nanostructures by de Boer *et al.* in the early 1990s [33]. Both techniques use similar measurements procedures, *i.e.* increasing the incidence angle and collecting data at various angles, and the same fundamental physical principles can be used to analyze the data. These are based on the same recursive Parratt's formalism [32], originally developed for XRR and more recently reformulated for GIXRF by de Boer [33]. Therefore, the two techniques can be run on the same experimental apparatus and the results analyzed together. Their combination allows a better characterization of the sample in terms of thickness, roughness, mass density and elemental profile. Furthermore, the use in conjunction of the electronic and the mass density profiles reduces the uncertainties of the individual methods [13].

It has been reported by Hönicke *et al.* [34-36] that is possible to use combined GIXRF-XRR analysis *via* a reference free method to quantitatively determine the elemental profile of a multilayers. This method, despite being very precise, can be run only at large scale facilities, where a complete knowledge and calibration of each individual instrumental component is possible.

Another possibility is using a reference-based method to access the quantitative elemental depth profile of unknown samples maintaining an adequate accuracy. Despite the fact that there are reports on the potentialities of this method [16, 35, 36], no actual (or practical ?)application of this approach is presently available in literature. The reference-based approach is very interesting because it is applicable not only at large facilities instruments, but also in laboratory with in-fab instruments where some instrumental parameters might be covered by the supplier's intellectual property. To implement a reference-based XRR-GIXRF, a set of well-known and characterized standard materials is essential. In the case of thin films nanotechnology, these references should respect specific requirements: i) the film should be of high quality, *i.e.* with a precise control of the composition and homogeneity; ii) the thickness of the layer should be comparable to that of the unknown specimen and in any case thin enough to avoid self-absorption phenomena; iii) should contain an exhaustive combination of elements present in the matrix of the specimens of interest. The main limitation of the diffusion of a reference-based approach is due to the scarcity of reference materials at the nanoscale.

In this work, we demonstrate the potentialities of a GIXRF-XRR combined strategy on a transition metal nitrides material and we present for the first time a quantitative elemental depth profile characterization using a reference-based method. Our results are compared with the results obtained using two destructive depth profiling techniques: Plasma Profiling Time-Of-Flight Mass Spectrometry (PP-TOF-MS) and Time-Of-Flight Secondary Ions Mass Spectrometry (TOF-SIMS) [37, 38].

## 2. Experimental

### 2.1 Sample preparation

Two different sample sets have been prepared at CEA-Leti laboratories: the first set, named the reference set, includes samples with well-known composition needed for the determination of the instrumental parameters required for reference-based GIXRF-XRR quantitative analysis; the second set, named the evaluation set, consists in a sample with unknown composition.

The reference set consists in two samples: a thin $Ti_{50}N_{50}$ layer and a thin $W_{50}N_{50}$ layer. The evaluation sample includes one $Ti_xW_yN$ thin layer of unknown composition. All the layers (with10 nm nominal thickness) were deposited on 200 mm silicon (001) substrates and capped in-situ with a 10 nm-thick amorphous carbon layer to avoid ageing effects.

All samples have been deposited by magnetron sputtering in Evatec Clusterline 200 industrial tool. The thin films were deposited from two distinct targets: titanium (purity 99.99%) and tungsten (purity 99.9%). Nitrogen was inserted *via* a gas mixture of Ar and $N_2$. A density of power of 0.4 to 2.5 $W.cm^{-2}$ was applied to Ti and W targets in order to tune the composition.

From each wafer, three samples of 2 cm x 4 cm (close to each other) were cut off. One specimen was used for PP-TOF-MS analysis, the second one for TOF-SIMS measurements and the last one for both Wavelength Dispersive X-Ray Fluorescence (WDXRF) and GIXRF-XRR combined analysis.

### 2.2 Instrumentation

In-line WDXRF experiments were carried out in the primary-vacuum chamber of a Rigaku AZX400 instrumentation (or spectrometer ?). The samples were irradiated with the polychromatic radiation of a rhodium X-ray tube operated at 45 kV and 75 mA. We used a LiF(200) crystal (2d = 4.027 A) mounted on a high-resolution goniometer to select the wavelengths related to Ti-Kα and W-Lα fluorescence lines. The intensity of Ti-Kα was recorded with a gas-flow type proportional counter, whereas W-Lα signal was measured using a scintillator. We applied the fundamental parameters approach [39], using pure titanium and tungsten –samples (or targets ?) to determine the spectrometer sensitivity values, in order to quantify the deposited mass of titanium and tungsten, then the Ti:W ratio in the TiWN thin materials. More details on the WDXRF calibration and uncertainties can be found in Supporting Information.

GIXRF-XRR combined measurements were acquired using a dedicated instrument, CASTOR, that has been developed by the Laboratoire National Henri Becquerel (CEA) [40] and that can be installed on the Metrology beamline at the French synchrotron SOLEIL (Saclay). The incoming beam was circularly shaped by a pinhole of diameter 400 (5) µm positioned at 0.995 m distance from the surface of the samples. . The analysis chamber is composed of a 7-axis goniometer allowing a fine alignment of the sample with respect to the incoming beam and its rotation during measurements. Two detectors complete the set-up: a photodiode to record the XRR signal in a theta/2theta configuration and a silicon drift detector (SDD) including a collimator to acquire the fluorescence one, placed at 90° with respect to the incoming beam. The chamber is maintained under a vacuum lower than $10^{-6}$ mbar. Details on XRR-GIXRF sample alignment procedure can be found in Supporting Information.

The GIXRF data have been acquired using two different incident energies of 6 keV and 10.5 keV, above the Ti-K edge and the W-L3 edge, respectively. These values are enough far from the white line to avoid possible effects of sharp changes of intensity in the NEXAFS region, while enough close to the edge to maximize the photon-electron coupling. The sample was rotated in the range 0° to 6° with a step of 0.005° during the measurement. The XRR signal have been recorded only at 6 keV and the sample rotated in the range 0° to 1.2° with a step of 0.005°.

Destructive Time of flight-secondary ion mass spectrometry (TOF-SIMS) depth profiles were acquired using an Ion Tof GmbH TOF-SIMS 5. $MCs^+$ analysis mode [41] (M being the element of interest) was chosen to limit matrix effects as much as possible. Sputtering was done using a 1 keV $Cs^+$ beam and analysis with a 25 keV $Bi_3^+$

primary beam. Both ion guns were incident on the sample surface at an angle of 45°. The sputtered craters were 300 x 300 µm² while the analysis zones were 80 x 80 µm² positioned at the center of the sputtering crater to avoid crater sidewall effects. Four shots per pixel were acquired in order to increase the counting statistics. In this analysis mode, a cesium rich environment is produced at the sample surface by cesium sputtering. Monitoring cesium adducts instead of monoatomic ions reduces the dependence of the secondary ions yields on the matrix material, and lowers artefacts at the interfaces.

Additional depth profiling was done using a Horiba Scientific Plasma Profiling Time of Flight Mass Spectrometry (PP-TOF-MS). The technique uses a pulsed radio frequency argon plasma for sample sputtering and ionization, coupled to an orthogonal time of flight mass spectrometer. When compared to TOF-SIMS, the technique is faster and exhibits limited matrix effects. Calibration-free semi-quantitative results have been obtained on a wide range of materials [16, 37, 42, 43]. Analysis conditions, namely plasma pressure and applied power, must be material-wise optimized in order to have a flat sputtering crater bottom and thus a good depth resolution. In this study we could not obtain plasma conditions delivering satisfying crater shapes for both the capping and the nitride materials. We selected the sputtering conditions leading to a flat crater bottom in the capping layer to preserve the depth resolution at the interface with the nitride layer. We used a 4mm diameter anode, the source pressure was set to 1.7 mbar and the applied power was 40 W. Pulsing period was 2000 µs with a pulse duration of 400 µs. Each point in the depth profiles corresponds to the average of the signals from 60 pulses. Depth profiles are presented in Ion Beam Ratio [44], which is the ratio of the ion currents weighed by their isotopic abundances.

### 2.3 Methodology

In this study, the GIXRF analysis have been performed using 6 keV and 10.5 keV energy for the incident beam. The choice of these measurement energies was made to be sufficiently above the absorption K-edge and the $L_3$-edge to have fluorescence yield from the elements of interest present in the system, i.e. 4.966 keV for the Ti and 10.207 keV for W, but close enough to avoid intensity losses due to inefficient X-ray-electron coupling. All fluorescence spectra were analyzed with the PyMca software [45] using batch processing, to obtain the dependence of the integrated intensity of each element of interest with respect to the incident angle. The background was simulated using a linear model before the batch processing.

Two methods are described in the literature to perform combined GIXRF-XRR data analysis. The first one, known as the “reference-free method”, is based on the calibration of the whole instrumentation in terms of detector efficiency, geometrical parameters, and incident beam intensity, shape and divergence [29, 46]. The second approach is the “reference-based method” [16]. It consists in the use of reference samples containing the same elements than the samples of interest to determine different instrumental parameters at each specific fluorescence emission line: the dimension of the detector collimator, the distance between the sample and the detector, and the detector response function. All these instrumental parameters were kept fix during the fit of GIXRF-XRR data of the unknown samples, while the thickness, roughness, mass density and stoichiometry were set as free parameters. All GIXRF and XRR data were processed using the home developed software MEDePY: Material Elemental Depth profiling using Python [47] for model simulation and fitting. More details on the XRR-GIXRF fitting procedure and MEDepy theoretical background and implementation can be found in Supplementary Materials.

## 3. Results and discussion

### 3.1 Analysis of the reference samples $Ti_{50}N_{50}$ and $W_{50}N_{50}$

We used WDXRF, TOF-SIMS and PP-TOF-MS analysis techniques to verify the elemental composition, the depth profile and possible cross-contamination of the reference samples, respectively.

The elemental composition of the films was determined by WDXRF and the results are reported in Table 1. Quantitative elemental analysis was performed using the fundamental parameter method [39] with relative sensitivity factors deduced from measurements of pure titanium and tungsten samples. WDXRF allowed a precise

determination of the samples composition with an absolute uncertainty on each elemental concentration close to 1.0 at. % (see Supporting Information for a more detailed discussion).

| Sample | Ti (at. %) | W (at. %) |
|---|---|---|
| $Ti_{50}N_{50}$ | 100 | 0 |
| $W_{50}N_{50}$ | 0 | 100 |
| $Ti_xW_yN$ | 20.4 | 79.6 |

**Table 1.** Quantitative analysis of the reference samples and the unknown sample $\pm$ 1 at%. For these samples, we did not estimate the nitrogen content as it would have required dedicated work to deal with the overlap between N-Kα (0.392 keV) and T-$L_l$ (0.395 keV) fluorescence lines.

TOF-SIMS measurements were instead carried out to evaluate potential interdiffusion between the capping and the nitride layer. Despite their shallow depths, the layers are well resolved as shown in Fig. 1. The observed gradients between $CCs_2^+$ and $MCs^+$ ions lie in the nanometer range, which is close to the depth resolution of the technique. We can then conclude that the elemental interdiffusion is not present or very limited into the samples. It worth noticing that the variation of the CsTi+ ion intensity at the interfaces is related to so called 'matrix effects' (dependence of the secondary ions yield over the local material composition). These effects are mitigated by using the MCs analysis method (following Cs adducts ions) but not completely removed.

We also used the TOF-SIMS measurements to evaluate nitrogen distribution in the nitride layers. As $N^+$ or $CsN^+$ ion intensities are too weak to be monitored in $MCs^+$ mode, we decided to use $CsTiN^+$ and $CsWN^+$ instead. The depth profiles obtained for $MCs^+$ and $MNCs^+$ ions are presented Fig. 2. $MCs^+$ and $MNCs^+$ ions vary in a similar way for both samples suggesting homogeneous nitrogen content. However, this indirect method does not allow for the quantification of nitrogen as a function of depth.
Due to its homogeneous sensitivity to a wide range of elements, PP-TOF-MS was favored over TOF-SIMS to evaluate a possible target cross-contamination during the deposition process. The technique has shown good abilities to detect contaminants in previous work [48].

The $Ti_{50}N_{50}$ sample did not evidence any tungsten contamination as no tungsten peak was observed in the layer-averaged mass spectra (not shown). For such counting statistics, ppm range sensitivity is expected. By contrast, for the sample $W_{50}N_{50}$, titanium isotopes were observed. The titanium contamination is low with an estimated atomic fraction of titanium over tungsten (Ion Beam Ratio method) of $3.10^{-4}$.

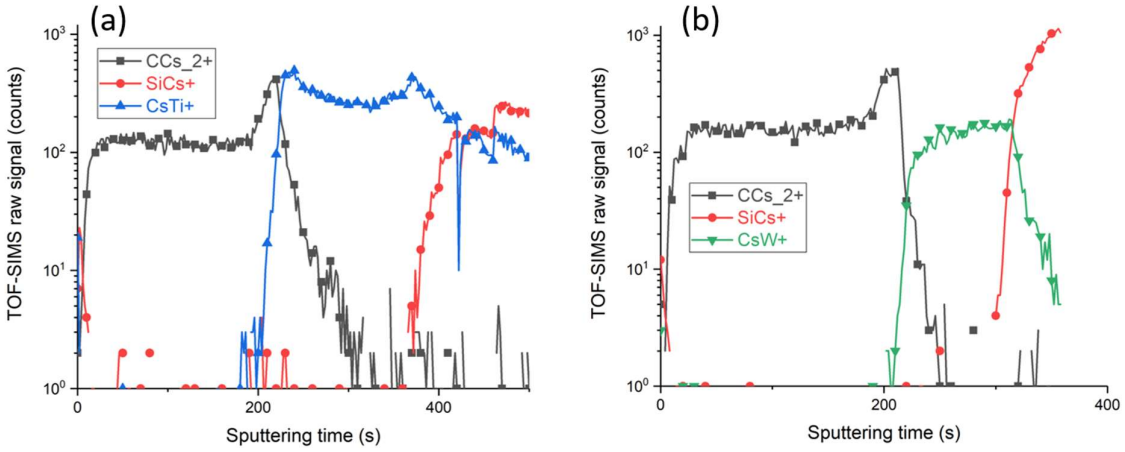


**Fig. 1.**
TOF-SIMS depth profiles of the reference samples $Ti_{50}N_{50}$ (a) and $W_{50}N_{50}$ (b), respectively.

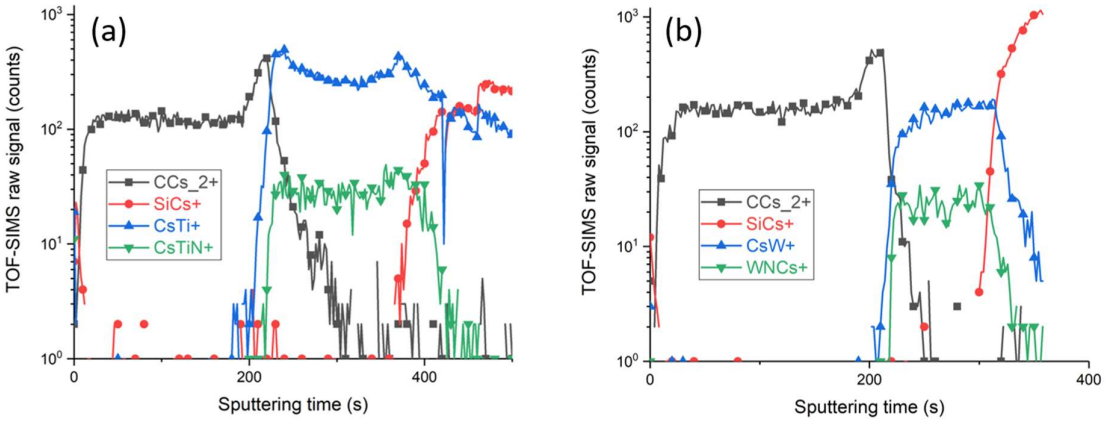


**Fig. 2.**

TOF-SIMS depth profiles of CsMN ions for $Ti_{50}N_{50}$ (a) and $W_{50}N_{50}$ (b) respectively.

All these measurements confirm that the reference samples $Ti_{50}N_{50}$ and $W_{50}N_{50}$ do not present any noticeable contamination and that there is not significant interdiffusion occuring at the layer/capping interface. This allows us to ascertain the validity of the elemental models of our references set and be sure of the accuracy of the calibration of the XRR-GIXRF with them.

We first modeled the XRR data of the reference set to retrieve initial values of thickness, mass density and roughness of the different layers (see Table 2). Then, we included the GIXRF data to perform the GIXRF-XRR combined analysis (see Fig. 3 and Table 2). All the physical parameters of the reference samples (thickness, roughness and mass density), and all the instrumental parameters (distance sample to XRF detector, detector pinhole height and pinhole width, detector quantum efficiency), were left free during the fitting process, whereas the elemental composition was fixed. The obtained refined instrumental parameters are reported in Table 3 and were used afterwards for the quantitative analysis of the unknown $Ti_XW_yN$ sample.

For the fit of reference samples, the uncertainties in the distances and sizes for the instrument parameters are in the range of few hundreds of µm or lower. More generally, relative uncertainties are all close or below 1%. The correlation matrix show for almost all of the parameters correlations below 10% and any correlation above 50%, suggesting that variables are independent and that we are not over interpreting data (see Table S1 in Supporting Information).

The uncertainties for the derived sample parameters are about few dozens of pm for the thickness, a few dozens of g/mm$^3$ for the density a few dozens of pm or the roughness. These uncertainties might not be pushed as the one possible with a reference-free method on a fully calibrated metrology beamline, but are enough accurate to consider results reliable and sufficiently precise.

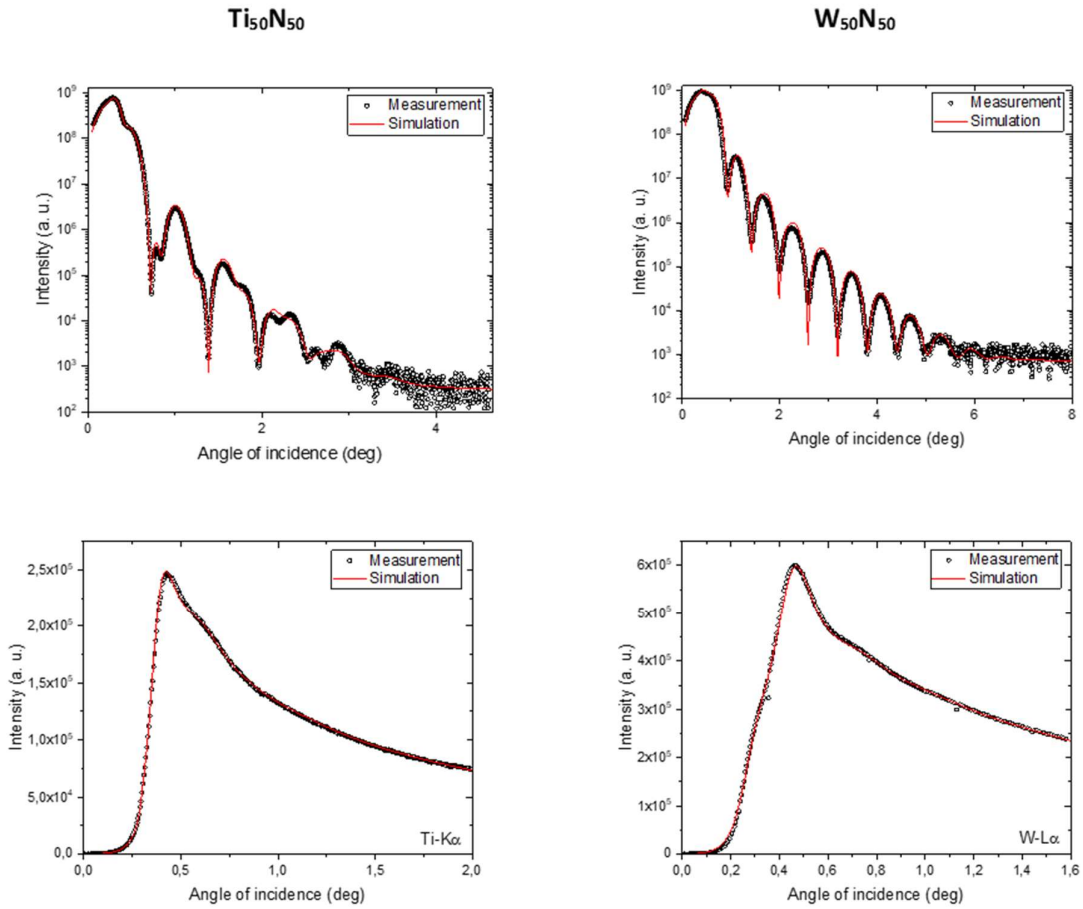


**Fig. 3.**
XRR-GIXRF measurements (black) and simulated curves (red) of the reference sample set. The instrumental parameters deduced from these fits are reported in Table 3.

| Sample name | Model | Layer | Thickness (nm) | ΔThickness (nm) | Density (g/cm3) | ΔDensity (g/cm3) | Roughness (nm) | ΔRoughness (nm) | Concentration (at.%) |
|---|---|---|---|---|---|---|---|---|---|
| $Ti_{50}N_{50}$ | XRR | C-capping | 12.30 | 0.02 | 1.610 | 0.017 | 0.780 | 0.004 | 100 |
| | | TiN-film | 9.29 | 0.01 | 5.150 | 0.026 | 0.884 | 0.002 | Ti50N50 |
| | | Si-substrate | // | // | 2.33 | // | 0.481 | 0.002 | 100 |
| | XRR-GIXRF | C-capping | 12.10 | 0.02 | 1.910 | 0.010 | 0.883 | 0.008 | 100 |
| | | TiN-film | 9.28 | 0.01 | 5.070 | 0.008 | 0.754 | 0.008 | Ti50N50 |
| | | Si-substrate | N/A | N/A | 2.33 | // | 0.470 | 0.003 | 100 |
| $W_{50}N_{50}$ | XRR | C-capping | 9.140 | 0.05 | 1.140 | 0.040 | 0.525 | 0.005 | 100 |
| | | WN-film | 9.470 | 0.004 | 13.700 | 0.105 | 0.343 | 0.004 | W50N50 |
| | | Si-substrate | // | // | 2.330 | | 0.250 | 0.001 | 100 |
| | XRR-GIXRF | C-capping | 9.530 | 0.05 | 1.8 | 0.00370 | 0.510 | 0.006 | 100 |
| | | TiN-film | 9.510 | 0.004 | 16.5 | 0.03070 | 0.370 | 0.004 | W50N50 |
| | | Si-substrate | // | // | 2.33 | // | 0.297 | 0.001 | 100 |

**Table 2**
Results issued from the XRR and GIXRF-XRR combined analysis, for both $Ti_{50}N_{50}$ and $W_{50}N_{50}$ reference samples.

| Parameter | | ±Δ |
|---|---|---|
| Beam width (µm) | 400 | |
| H1 (mm) | 24.64 | 0.27 |
| Pressure (Pa) | 10^-6 | |
| Resolution (deg) | 0.005 | |
| H2 (mm) | 0.65 | 0.01 |
| D1 (mm) | 3.04 | 0.06 |
| Quantum detector efficiency Ti-Kα | 42 | 4 |
| Quantum detector efficiency W-Lα | 3.05 | 0.21 |

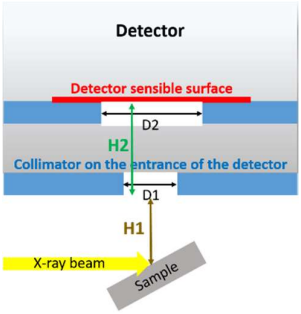


**Table 3**
Instrumental parameters obtained from the GIXRF-XRR combined analysis of the references samples $Ti_{50}N_{50}$ and $W_{50}N_{50}$. These parameters were then used for the GIXRF-XRR combined analysis performed on the $Ti_XW_yN$ sample.

### 3.2 Analysis of the unknown $Ti_XW_YN$ sample

We started the fitting procedure of $Ti_XW_yN$ sample with the model obtained from a preliminary XRR analysis alone, using the previously determined instrumental parameters shown in Table 3 that were kept fixed during the fits. The physical parameters of the unknown thin films are summarized in Table 4 (XRR model) and were used as initial values for the combined GIXRF-XRR analysis.

Both the GIXRF and XRR are reasonably represented by a simple bilayer model, which only includes the carbon capping layer and the TiWN thin layer (Fig. 4 and Table 4) (GIXRF-XRR model). However, slight discrepancies can be seen between the data and the best-model calculation on both GIXRF XRR curves (see arrows in Fig. 4.), thereby suggesting an in-depth elemental profile in the $Ti_xW_yN$ layer (see also Table S2 in Supporting Information for the correlation matrix). To be sure that uncertainties in the instrumental parameter could not be the responsible for such a discrepancy, we modeled the XRR and GIXRF curves using instrument parameters away from those reported in Table 3 by a factor 2σ. The results are reported in Figure S1 in Supporting Information and show that the uncertainty on instrument parameters cannot account for the discrepancies present in the bottom layers of Figure 4.

| Sample name | Model | Layer | Thickness (nm) | Δ Thickness (nm) | Density (g/cm3) | Δ Density (g/cm3) | Roughness (nm) | Δ Roughness (nm) | Concentration (at.%) |
|---|---|---|---|---|---|---|---|---|---|
| TixWyN | XRR | C-capping | 9.01 | 0.07 | 0.92 | 0.04 | 0.417 | 0.026 | 100 |
| | | TiWN-film | 9.380 | 0.004 | 11.90 | 0.09 | 0.356 | 0.005 | TixWyN |
| | | Si-substrate | // | // | 2.33 | // | 0.2500 | 0.0004 | 100 |
| | XRR-GIXRF | C-capping | 11.50 | 0.20 | 2.07 | 0.05 | 0.437 | 0.019 | 100 |
| | | TiWN-film | 9.32 | 0.03 | 12.40 | 0.01 | 0.304 | 0.006 | Ti0.62W1.84N |
| | | Si-substrate | // | // | 2.33 | // | 0.318 | 0.010 | 100 |
| | XRR-GIXRF multilayer | C-capping | 11.30 | 0.04 | 1.98 | 0.02 | 0.511 | 0.008 | 100 |
| | | TiWN-film | 0.883 | 0.007 | 13.20 | 0.18 | 0.320 | 0.002 | Ti0.32W0.77N |
| | | TiWN-film | 7.98 | 0.17 | 13.30 | 0.06 | 0.307 | 0.008 | Ti0.20W0.62N |
| | | TiWN-film | 0.595 | 0.008 | 9.77 | 0.25 | 0.385 | 0.007 | Ti0.14W0.70N |
| | | Si-substrate | // | // | 2.33 | // | 0.200 | 0.010 | 100 |

**Table 4**
Fitting results of the data using the different models: XRR monolayer, GIXRF-XRR monolayer and PP-TOF-MS tri-layer.

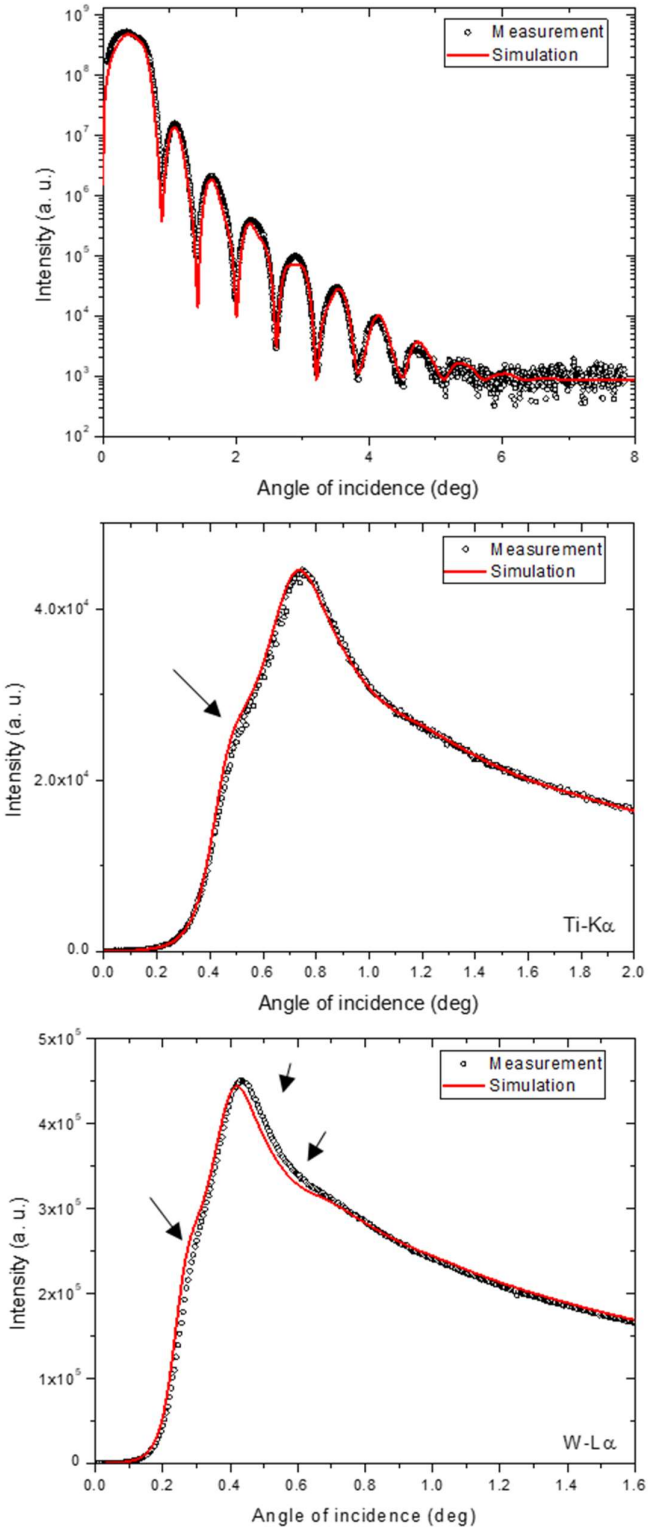


**Fig. 4.**

GIXRF-XRR measurements (black line) and simulated curves (red points) using the GIXRF-XRR combined analysis and the instrumental parameters reported in the Table 3.

In order to evaluate this hypothesis, PP-TOF-MS and MCs+ TOF-SIMS analyses were also performed on the unknown sample. Depth profiles of the ternary sample analyzed using both techniques are presented in Fig. 5, which also displays the relative composition of titanium and tungsten in the nitride layer. Relative Sensitivity Factors (RSF) were applied to match WDXRF estimated average composition. PP-TOF-MS has the advantage of a similar sensitivity to titanium and tungsten, while TOF-SIMS, although not as sensitive to tungsten with respect to titanium, achieves a better depth resolution. Both techniques show gradients in the nitride layer with a relatively higher titanium content at the capping / nitride layer interface and a relatively higher tungsten content at the nitride / substrate interface. As a consequence, a three sub-layers model seems more appropriate to represent the titanium and tungsten distribution in the nitride layer than the homogeneous one previously proposed.

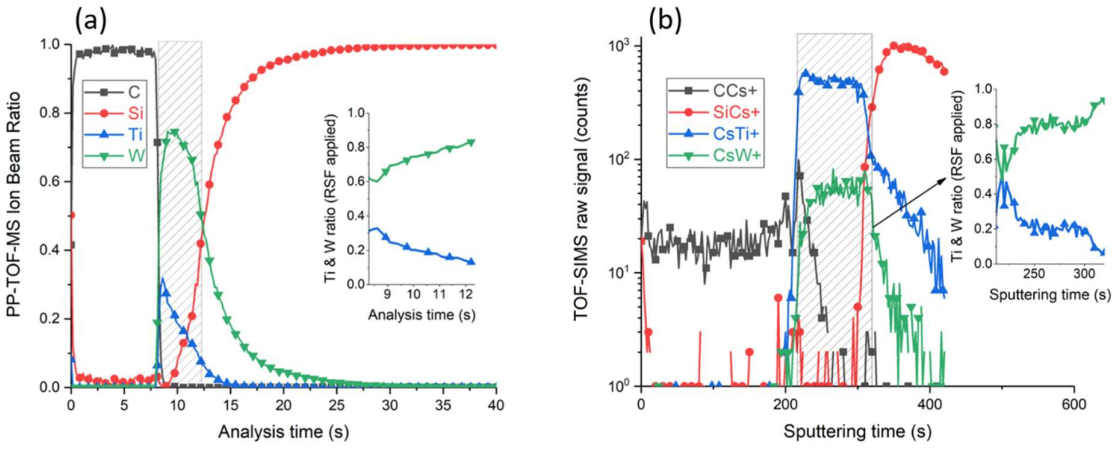


**Fig. 5.**
Depth profiles of capped sample obtained using (a) PP-TOF-MS and (b) TOF-SIMS. Insets present the estimated relative composition of titanium and tungsten in the outlined nitride layer.

We integrated the elemental profile suggested by the PP-TOF-MS/TOF-SIMS analysis in the refined GIXRF-XRR model, in which the sample thickness was subdivided in three discrete thin layers. The thickness, mass density, roughness and elemental concentration of titanium, tungsten and nitrogen were left as free parameters in all the three layers and their values deduced by the combined GIXRF-XRR fit. The recorded data and the fitted curves of the combined analysis of multilayer model (see Fig. 6 and Table 4 (XRR-GIXRF)) highlight the benefit of the introduction of a compositional gradient. The GIXRF-XRR analysis pointed out the following general trend in the TiWN layer: i) at the capping-film interface, there is a thin layer of 0.9 nm showing a large concentration of titanium; ii) a second thicker layer is characterized by a stoichiometry rich in tungsten; iii) a thin third layer still richer in tungsten, but accompanied by a lower titanium content respect to the previous one. The total thickness of the TiWN layer is equal to the value found by the XRR analysis.

Covariance matrix analysis showed, to the exception, correlations below 10% among parameters (see Table S3 in supporting Information). It is true that we have the largest correlation (~40%) between the density and the thickness of each layer in the 3-layers model. This results induces (?) a lower accuracy in the determination of one or the other parameter (see Table 4) in each layer, remaining however reasonably precise.

The analysis of $Ti_XW_yN$ allowed in the end the definition of the following stoichiometry in the three modeled layers (from top to bottom): i) $Ti_{0.32}W_{0.77}N$; ii) $Ti_{0.20}W_{0.62}N$; iii) $Ti_{0.14}W_{0.7}N$. All the parameters retrieved from the combined GIXRF-XRR analysis are reported Table 4.

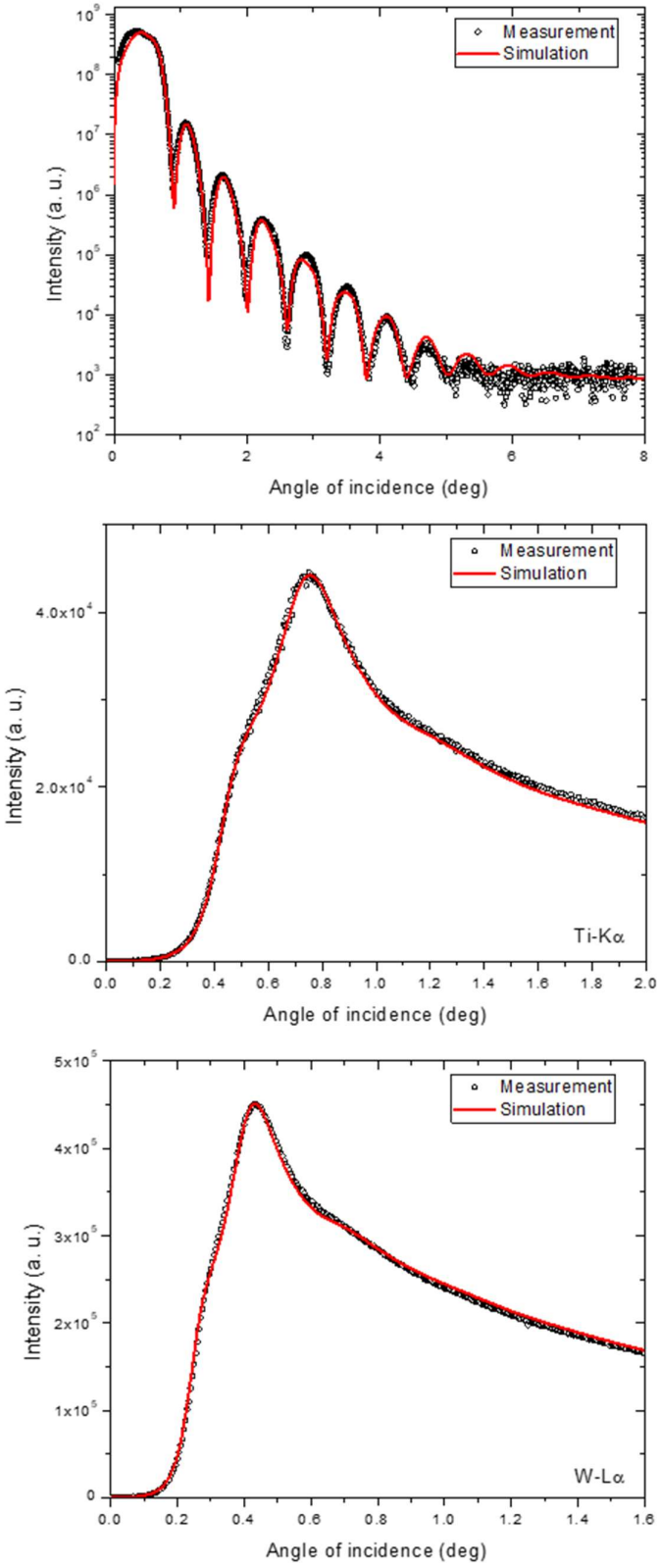


**Fig. 6.**
GIXRF-XRR measurements (black points) and simulated curves (red line) using the GIXRF-XRR combined analysis, the instrumental parameters reported in the Table 3 and the model suggested by PP-TOF-MS analysis.

## 4. Conclusions

In this study, we demonstrated that reference-based GIXRF-XRR combined analysis can meet the need for non-destructive quantitative depth-profiling of complex transition metal nitride thin materials. This reference-based methodology relies on the use of reference (or at least well-known) samples, which contain the same elements than the unknown samples, in order to determine the instrumental function of the setup. We used this methodology to reveal small titanium depth-profile in the 0.9 nm upper part of a 10 nm-thick TiWN layer. This titanium profile was confirmed by destructive techniques based on time-of-flight mass spectrometry (PP-TOFMS and TOF-SIMS). Reference-based GIXRF-XRR could therefore be propagated to lab and fab tools so as to allow for non-destructive quantitative depth-profiling in industrial process control schemes.

## Acknowledgements

This work was funded through the European Metrology Programme for Innovation and Research (EMPIR) Project 16ENG03 HyMet. The EMPIR is jointly funded by the EMPIR participating countries within European Association of National Metrology Institutes (EURAMET e.V., Braunschweig Germany) and the European Union.

We acknowledge SOLEIL for provision of synchrotron radiation facilities and we would like to thank to thank Pascal Mercere and Paulo Da Silva for assistance in using the Metrology beamline and for all useful discussions. Also, we thank Giancarlo Pepponi (FBK) for useful discussion about combined GIXRF-XRR data analysis and lastly, we thank Jean-Paul Barnes from Leti for interesting discussion about the TOF-SIMS and PP-TOF-MS measurements.

TOF-SIMS measurements were performed at the Nanocharacterization Platform (PFNC) of the CEA Grenoble.

## References

[1] C. S. Lee, E.Y. Chang, L. Chang, C.Y. Fang, Y.L. Huang, J.S. Huang, Study of Titanium Tungsten Nitride and Tungsten Nitride Schottky Contacts on n-GaN, Jpn. J. Appl. Phys. 42 (2003) 4193-4196. https://doi.org/10.1143/JJAP.42.4193.

[2] Lin, K. C.; Chang, E. Y.; Wang, S. P.; Lai, Y. L.; Chang, C. Y., TIWN SCHOTTKY CONTACTS TO N-GA(0.51)IN(0.49)P. Jpn. J. Appl. Phys. Part 1 - Regul. Pap. Short Notes Rev. Pap. 1994, 33 (8), 4546-4549.

[3] Geissberger, A. E.; Sadler, R. A.; Balzan, M. L.; Crites, J. W., TIW NITRIDE THERMALLY STABLE SCHOTTKY CONTACTS TO GAAS - CHARACTERIZATION AND APPLICATION TO SELF-ALIGNED GATE FIELD-EFFECT TRANSISTOR FABRICATION. J. Vac. Sci. Technol. B 1987, 5 (6), 1701-1706.

[4] Wu, H. D.; Huang, W.; Lu, W. F.; Tang, R. F.; Li, C.; Lai, H. K.; Chen, S. Y.; Xue, C. L., Ohmic contact to n-type Ge with compositional Ti nitride. Appl. Surf. Sci. 2013, 284, 877-880.

[5] Wu, H. D.; Wang, C.; Wei, J. B.; Huang, W.; Li, C.; Lai, H. K.; Li, J.; Liu, C.; Chen, S. Y., Ohmic Contact to n-Type Ge With Compositional W Nitride. IEEE Electron Device Lett. 2014, 35 (12), 1188-1190.

[6] C. C. Tan, R. Zhao, L. Shi, T. C. Chong**,** Implementation of nitrogen-doped titanium-tungsten tunable heater in phase change random access memory and its effects on device performance**,** Applied Physics Letters 105 (2014) 153501. https://doi.org/10.1063/1.4898002.

[7] Zhou, S.; Liu, W. G.; Liu, H.; Cai, C. L.; Qin, W. G.; Guo, F., TiWN resistive films in an infrared scene projector device and the array fabrication. In International Symposium on Photoelectronic Detection and Imaging 2011: Sensor and Micromachined Optical Device Technologies, Wang, Y.; Xie, H.; Jin, Y., Eds. Spie-Int Soc Optical Engineering: Bellingham, 2011; Vol. 8191.

[8] Uchibori, C. J.; Ohtani, Y.; Oku, T.; Ono, N.; Murakami, M., InxGa1-xAs-based Ohmic contacts to n-type GaAs with W-nitride barrier prepared by radio frequency sputtering. Appl. Surf. Sci. 1997, 117, 347-351.

[9] Raaijmakers, I. J.; Setalvad, T.; Bhansali, A. S.; Burrow, B. J.; Gutai, L.; Kim, K. B., MICROSTRUCTURE AND BARRIER PROPERTIES OF REACTIVELY SPUTTERED TI-W NITRIDE. J. Electron. Mater. 1990, 19 (11), 1221-1230.

[10] Hong, S. H.; O'Sullivan, J.; Jonsson, M.; Rimmer, N., Improvements in TiWN barrier technology for devices using Au metallisation. Microelectron. Eng. 2002, 64 (1-4), 329-334.

[11] A. G. Dirks, R. A. M. Wolters, A. J. M. Mitchell, Thin solid Films 53 (1978) 195.

[12]J. Lubeck, B. Beckhoff, R. Fliegauf, I. Holfelder, P. Hönicke, M. Müller, B. Pollakowski, F. Reinhardt, J. Weser, A novel instrument for quantita-tive nanoanalytics involving complementary X-ray methodologies, Rev. Sci. Instrum. 84 (2013) 045106. http://dx.doi.org/10.1063/1.4798299

[13] Ingerle, D.; Meirer, F.; Pepponi, G.; Demenev, E.; Giubertoni, D.; Wobrauschek, P.; Streli, C., Combined evaluation of grazing incidence X-ray fluorescence and X-ray reflectivity data for improved profiling of ultra-shallow depth distributions. Spectroc. Acta Pt. B-Atom. Spectr. 2014, 99, 121-128.
[14] Ingerle, D.; Schiebl, M.; Streli, C.; Wobrauschek, P., Combination of grazing incidence x-ray fluorescence with x-ray reflectivity in one table-top spectrometer for improved characterization of thin layer and implants on/in silicon wafers. Rev. Sci. Instrum. 2014, 85 (8), 5.
[15] B. Caby, F. Brigidi, D. Ingerle, E. Nolot, G. Pepponi, C. Streli, L. Lutterotti, A. André, G. Rodriguez, P. Gergaud, M. Morales, D. Chateigner, Study of annealing-induced interdiffusion in In2O3/Ag/In2O3 structures by a combined X-ray reflectivity and grazing incidence X-ray fluorescence analysis, Spectrochimica Acta, Part B 113 (2015) 132–137. http://dx.doi.org/10.1016/j.sab.2015.09.008.
[16] H. Rotella, B. Caby, Y. Ménesguen, Y. Mazel, A. Valla, D. Ingerle, B. Detlefs, M.-C. Lépy, A. Novikova, G. Rodriguez, C. Streli, E. Nolot, Elemental depth profiling in transparent conducting oxide thin film by X-ray reflectivity and grazing incidence X-ray fluorescence combined analysis, Spectrochimica Acta Part B 135 (2017) 22-28. http://dx.doi.org/10.1016/j.sab.2017.06.011
[17] Maderitsch, A.; Ingerle, D.; Bretschneider, T.; Rauwolf, M.; Pflumm, C.; Buchholz, H.; Borchert, H.; Streli, C.; Parisi, J., Analysis of organic multilayer structures using a combined grazing incidence X-ray fluorescence/X-ray reflectometry approach. Spectroc. Acta Pt. B-Atom. Spectr. 2018, 148, 188-192.
[18] E. Nolot, B. Caby, R. Gassilloud, M. Veillerot, D. Eichert, X-ray reflectometry and grazing-incidence X-ray fluorescence characterization of innovative electrodes for tantalum-based resistive random access memories, Spectrochimica Acta, Part B, 149 (2018) 71-75. https://doi.org/10.1016/j.sab.2018.07.017.
[19] W. Pessoa, A. Roule, E. Nolot, Y. Mazel, M. Bernard, M.-C. Lépy, Y. Ménesguen, A. Novikova, P. Gergaud, F. Brigidi, D. Eichert, Grazing incident X-ray fluorescence combined with X-ray reflectometry metrology protocol of telluride-based films using in-lab and synchrotron instruments, Spectrochimica Acta, Part B, 149 (2018) 143-149. https://doi.org/10.1016/j.sab.2018.07.003.
[20] Honicke, P.; Detlefs, B.; Nolot, E.; Kayser, Y.; Muhle, U.; Pollakowski, B.; Beckhoff, B., Reference-free grazing incidence x-ray fluorescence and reflectometry as a methodology for independent validation of x-ray reflectometry on ultrathin layer stacks and a depth-dependent characterization. J. Vac. Sci. Technol. A 2019, 37 (4), 6.
[21] Trivedi, A.; Rao, P. N.; Choudhary, R. J.; Tiwari, M. K., Determination Of Arsenic Diffusion In PLD Grown ZnO Thin Films Using Synchrotron Based XRR-GIXRF Measurements. In Dae Solid State Physics Symposium 2018, Biswas, A.; Sharma, V. K.; Yusuf, S. M., Eds. Amer Inst Physics: Melville, 2019; Vol. 2115.
[22] D. Ingerle, G. Pepponi, F. Meirer, P. Wobrauschek, C. Streli, JGIXA - A software package for the calculation and fitting of grazing incidence X-ray fluorescence and X-ray reflectivity data for the characterization of nanometer-layers and ultra-shallow-implants, Spectrochimica Acta B 118 (2016) 20–28. https://doi.org/10.1016/j.sab.2006.12.002.
[23] J. Als-Nielsen, D. McMorrow, Elements of Modern X-ray Physics, Wiley, 2011.
[24] Chason, E.; Mayer, T. M., Thin film and surface characterization by specular X-ray reflectivity. Critical Reviews in Solid State and Materials Sciences 1997, 22 (1), 1-67.
[25] R. Unterumsberger, B. Pollakowski, M. Muller, B. Beckhoff, Complementary characterization of buried nanolayers by quantitative X-ray fluorescence spectrometry under conventional and grazing incidence conditions, Anal. Chem. 83 (2011) 8623-8628. https://doi.org/10.1021/ac202074s.
[26] P. Honicke, B. Beckhoff, M. Kolbe, D. Guibertoni, J. A. van den Berg, and G. Pepponi Depth profile characterisation of ultra shallow junction implants, Anal. Bioanal. Chem. 396(8) (2010) 2825-2832. https://doi.org/10.1007/s00216-009-3266-y
[27] B. Pollakowski, B. Beckhoff, F. Reinhardt, S. Braun, and P. Gawlitza, Speciation of deeply buried TiOx nanolayers with grazing-incidence x-ray fluorescence combined with a near-edge x-ray absorption fine-structure investigation, Phys. Rev. B 77 (2008) 235408. https://doi.org/10.1103/PhysRevB.77.235408
[28] M. Müller, P. Hönicke, B. Detlefs, and C. Fleischmann, Characterisation of high-k nanolayers by grazing incidence X-ray spectrometry, Materials, 7, (2014) 3147-3159. https://doi.org/10.3390/ma7043147.
[29] Honicke, P.; Detlefs, B.; Muller, M.; Darlatt, E.; Nolot, E.; Grampeix, H.; Beckhoff, B., Reference-free, depth-dependent characterization of nanolayers and gradient systems with advanced grazing incidence X-ray fluorescence analysis. Phys. Status Solidi A-Appl. Mat. 2015, 212 (3), 523-528.
[30] M. Krämer, A. von Bohlen, C. Sternemann, M. Paulus, and R. Hergenröder, Synchrotron radiation induced X-ray standing waves analysis of layered structures, Appl. Surf. Sci. 253 7 (2007) 3533-3542. https://doi.org/10.1016/j.apsusc.2006.07.076.
[31] A. von Bohlen, Total reflection X-ray fluorescence and grazing incidence X-ray spectrometry - tools for micro- and surface analysis, Spectrochim. Acta, Part B 64 (2009) 821–832. http://dx.doi.org/10.1016/j.sab.2009.06.012.
[32] L. G. Parratt, Surface studies of solids by total reflection of X-rays, Phys. Rev 95 (1954) 359–369. http://dx.doi.org/10.1103/PhysRev.95.359.

[33] D.K.G de Boer, Glancing-incidence X-ray fluorescence of layered materials,Phys. Rev. B 44 (1991) 498–511. http://dx.doi.org/10.1103/PhysRevB.44.498.
[34] C. Streeck, S. Brunken, M. Gerlach, C. Herzog, P. Hönicke, C. A. Kaufmann, J. Lubeck, B. Pollakowski, R. Unterumsberger, A. Weber, B. Beckhoff, B. Kanngießer, H.-W. Schock, and R. Mainz, Grazing-incidence x-ray fluorescence analysis for non-destructive determination of In and Ga depth profiles in Cu(In,Ga)Se2 absorber films, Applied Physics Letters 103 11 (2013) 1139041-1139045. https://doi.org/10.1063/1.4821267.
[35] P. Hönicke, B. Detlefs, M. Müller, E. Darlatt, E. Nolot, H. Grampeix, B. Beckhoff, Reference-free, depth-dependent characterization of nanolayers and gradient systems with advanced grazing incidence X-ray fluorescence analysis, Phys. Status Solidi A 212 3 (2015) 523-528. https://doi.org/10.1002/pssa.201400204.
[36] P. Hönicke1, B. Detlefs, E. Nolot, Y. Kayser, U. Mühle, B. Pollakowski, B. Beckhoff, Reference-free grazing incidence x-ray fluorescence and reflectometry as a methodology for independent validation of x-ray reflectometry on ultrathin layer stacks and a depth-dependent characterization, Journal of Vacuum Science & Technology A **37** (2019) 0415021-0415026. https://doi.org/10.1116/1.5094891.
[37] A. Tempez, S. Legendre, J.-P. Barnes and E. Nolot Combining plasma profiling TOFMS with TOF-SIMS depth profiling for microelectronic applications J. Vac. Sci. Technol. B 34 (2016) 03H120. https://doi.org/10.1116/1.4943513.
[38] Y. Mazel, E. Nolot, J.-P. Barnes, M. Charles, R. Bouveyron, M. Mrad, A. Tempez and S. Legendre, Multitechnique elemental depth profiling of InAlGaN and InAlN films J. Vac. Sci. Technol. B 36 (2018) 03F119. https://doi.org/10.1116/1.5019635.
[39] M. Mantler, J.P Willis, G.R Lachance, B.A.R Vrebos, K.E Mauser, N. Kawahara, R.M Rousseau, P.N Brouwer, B. Beckhoff, B. Kanngiesser, N. Langhoff, R. Wedell, H. Wolff, H., Handbook of Practical X-Ray Fluorescence Analysis, Eds.; Springer: Berlin, Germany, 2006; pp. 309–410.
[40] Y. Ménesguen B. Boyer H. Rotella J. Lubeck J. Weser B. Beckhoff D. Grötzsch B. Kanngießer , A. Novikova E. Nolot M.-C. Lépy, CASTOR, a new instrument for combined XRR-GIXRF analysis at SOLEIL, X-Ray Spectrom. 46 (2017) 303–308. https://doi.org/10.1002/xrs.2742.
[41] K. Chu, Y. Gao and J. W. Erickson, Characterization of III nitride materials and devices by secondary ion mass spectrometry J. Vac. Sci. Technol. B 16 (1998) 197. https://doi.org/10.1116/1.589777.
[42] Y. Canvel, S. Lagrasta, C. Boixaderas, S. Barnola, Y. Mazel and E. Martinez, Study of Ge-rich GeSbTe etching process with different halogen plasmas, J. Vac. Sci. Technol. A 37 (2019) 0313021-0313029. https://doi.org/10.1116/1.5089037.
[43] M. Mrad, Y. Mazel, J. Kanyandekwe, R. Bouveyron, G. Feuillet and M. Charles Solving the problem of gallium contamination problem in InAlN layers in close coupled showerhead reactors**,** Appl. Phys. Express 12 (2019) 0455041-0455044. https://doi.org/10.7567/1882-0786/ab0bbb.
[44] F. L. King, J. Teng and R. E. Steiner, Glow discharge mass spectrometry: Trace element determinations in solid samples, J. Mass Spectrom. 30 (1995) 1061-1075. https://doi.org/10.1002/jms.1190300802.
[45] V. Solé, E. Papillon, M. Cotte, P. Walter, J. Susini, A multiplatform code for the analysis of energy-dispersive X-ray fluorescence spectra, Spectrochim. Acta B At. Spectrosc. 62 (2007) 63–68. https://dx.doi.org/10.1016/j.sab.2006.12.002.
[46] B. Beckhoff, Reference-free X-ray spectrometry based on metrology using synchrotron radiation, J. Anal. Spectrom 23 (2008) 845-853. http://dx.doi.org/10.1039/B718355K.
[47] E. Nolot, G. Picot, D. Blanka, H. Rotella, S. Torrengo, Y. Mazel MEDEePY: Material Elemental DEpth profiling using PYton, in progress.
[48] Y. Mazel, J.-P. Barnes, E. Nolot, A. Tempez, and S. Legendre, 28th Annual SEMI Advanced Semiconductor Manufacturing Conference (2017) 285–288. http://dx.doi.org/10.1109/ASMC.2017.7969245.